Check for updates

Behavior and Design Aspects of FRP-Strengthened URM Walls under Out-of-Plane Loading

H. M. Elsanadedy[1]; Y. A. Al-Salloum[2]; Z. M. Al-Zaheri[3]; S. H. Alsayed[4]; and H. Abbas, M.ASCE[5]

Abstract: The use of externally bonded fiber-reinforced polymer (FRP) composites for upgrading the out-of-plane flexural resistance of unreinforced masonry (URM) walls is experimentally and analytically investigated in this study. A total of six hollow concrete block walls were tested to failure using an airbag and a reaction frame to obtain a uniform load on the wall. The masonry walls were placed horizontally and tested as one-way slabs with span direction perpendicular to the bed joints. The first wall was left unstrengthened to be used as control specimen; the other five walls were strengthened using different schemes of externally attached glass-fiber-reinforced polymer (GFRP) sheets. The main parameters studied experimentally were FRP reinforcement ratio and stiffness. In addition to the experimental program, an analytical model was developed to predict the ultimate moment capacity of the URM walls. The procedure outlined in standard guidelines was also utilized to compute the flexural capacity of walls. Besides the URM wall specimens tested in this study, another 42 test results of URM walls available in literature were used for analytical model validation. A design model was also proposed and new design aspects were introduced. **DOI: 10.1061/(ASCE)CC.1943-5614.0000695.** *© 2016 American Society of Civil Engineers.*

Author keywords: Masonry wall; Out-of-plane behavior; Fiber-reinforced polymer (FRP); Flexural strengthening; Analytical modeling.

Downloaded from ascelibrary.org by King Saud University on 01/12/21. Copyright ASCE. For personal use only; all rights reserved.

Introduction

Generally, buildings built with unreinforced masonry (URM) walls perform poorly in seismic events. The URM walls usually failed due to out-of-plane bending stresses resulting from seismic inertial forces. Another failure mode is related to the in-plane shear behavior in which the URM walls act as a part of the lateral load resisting system of the URM building.

The last few decades have seen the emergence of fiber-reinforced polymer (FRP) composites as a successful strengthening material for a wide range of construction applications including the retrofitting of timber, steel, and reinforced concrete (RC) structures (Mosallam 2002). Numerous studies have been carried out for evaluating the use of FRP laminates for repair and retrofitting of URM walls subjected to lateral loading (Triantafillou 1998; Hamoush et al. 2001; Kuzik et al. 2003; Tumialan et al. 2003a, b; Tan and Patoary 2004; Ghobarah and Galal 2004; El-Dakhakhni et al. 2006; Lunn and Rizkalla 2011). The benefits of using FRP composites for the retrofitting of URM walls are (1) high corrosion resistance and high strength-to-weight ratio of FRP, (2) no alterations in the architectural and geometrical configuration of the walls, and (3) ease of installation.

Many investigators have used externally bonded FRP strips for the retrofitting of URM walls against out-of-plane static loads and found these to be effective in increasing the load-carrying capacity. Velazquez-Dimas et al. (2000) used glass fiber-reinforced polymer (GFRP) strips for the strengthening of single-wythe and double-wythe masonry walls. The walls were tested under cyclic out-of-plane loads. The single-wythe walls failed in tension, excessive delamination, or a combination of both whereas the double-wythe walls failed by peeling off of composite strips and splitting of the wythes. They reported significant improvement in the strength and deformation capacity of the retrofitted walls. Albert et al. (2001) tested FRP-strengthened full-scale masonry walls under out-of-plane flexural loads. The FRP was found to improve the load-carrying capacity of masonry walls. Hamilton and Dolan (2001) used GFRP for the strengthening of wall against out-of-plane loads. The experiments showed that the FRP laminates can be successfully used for the retrofitting of unreinforced and underreinforced masonry walls. The flexural strength design equations were proposed that overpredicted the experimental results of test specimens by up to 20%. Hamoush et al. (2001) conducted out-of-plane static load tests on scaled masonry walls strengthened using different configurations of FRP strips. The distributed lateral load was applied using an airbag (ASTM 2014). They concluded that the flexural capacity of URM masonry walls can be increased by controlling the shear failure of walls. Dafnis et al. (2002) performed shake-table tests on full-scale infill masonry walls under simulated transient seismic loads. Finite-element analysis was used to satisfactorily simulate the test results. The arching action was observed in the walls confined between rigid frames, which significantly improved the flexural resistance of wall to lateral loads. Tumialan et al. (2003b) studied experimentally the flexural behavior of FRP-strengthened masonry walls using different amounts and types of FRP reinforcement. The effect of the putty filler on the bond strength was also studied. They provided a design approach for the retrofitting of masonry walls with FRP sheets. Al-Salloum and Almusallam (2005) and Almusallam and Al-Salloum (2007) used

[1]Associate Professor, Dept. of Civil Engineering, King Saud Univ., Riyadh, Saudi Arabia 11421. E-mail: helsanadedy@ksu.edu.sa

[2]Professor, Chair for Research and Studies in Strengthening and Rehabilitation of Structures, Dept. of Civil Engineering, King Saud Univ., Riyadh, Saudi Arabia 11421. E-mail: ysalloum@ksu.edu.sa

[3]Graduate Student, Dept. of Civil Engineering, King Saud Univ., Riyadh, Saudi Arabia 11421.

[4]Professor, Dept. of Civil Engineering, King Saud Univ., Riyadh, Saudi Arabia 11421.

[5]Professor, Chair for Research and Studies in Strengthening and Rehabilitation of Structures, Dept. of Civil Engineering, King Saud Univ., Riyadh, Saudi Arabia 11421 (corresponding author). E-mail: abbas_husain@hotmail.com

Note. This manuscript was submitted on October 6, 2015; approved on January 29, 2016; published online on May 3, 2016. Discussion period open until October 3, 2016; separate discussions must be submitted for individual papers. This paper is part of the ***Journal of Composites for Construction***, © ASCE, ISSN 1090-0268.

FRP laminates for strengthening of the concrete block walls against out-of-plane and in-plane loads, reporting considerable strength enhancement in all GFRP-retrofitted test specimens. The researchers proposed simplified design equations to estimate the flexural strength of retrofitted masonry walls. Hrynyk and Myers (2008) tested retrofitted infill masonry walls under static out-of-plane loads. The arching mechanism was reported in the failure of walls, and the authors reported the effectiveness of polyurea spray on walls in enhancing wall's energy absorption and decreasing flying debris. The premature failure of infill walls strengthened with a combination of polyurea and GFRP strips was attributed to the lack of anchorage between the retrofitted walls and the frame. An analytical model was developed to assess the ultimate flexural capacity of the retrofitted walls. Valluzzi et al. (2014) conducted experiments to study the performance of different FRP and textile-reinforced mortar (TRM) strengthening schemes for hollow masonry panels against out-of-plane loads. The test specimens were tested against out-of-plane loads using four-point flexure tests. Moment–curvature analysis provided approximate bilinear curves representing the bending behavior of panels.

This paper investigates experimentally and analytically the influence of FRP reinforcement ratio and FRP stiffness on the response and failure modes of FRP-strengthened URM walls against out-of-plane loading. A total of six hollow concrete masonry walls were tested under uniform loading applied via an airbag. Analytical modeling was also conducted to predict the load capacity of walls. In addition to the six walls tested in this study, another 42 walls (3 unstrengthened + 39 strengthened) were collected from the literature for model verification. The novelty of this study is that a fairly large database of 43 FRP-strengthened URM walls with different parameters, e.g., type of masonry, FRP reinforcement ratio, and FRP stiffness, are used for analytical model verification. Based on the validation of test results, a design model is proposed and new design aspects are introduced.

Experimental Program

Test Matrix

The experimental program is planned to investigate the feasibility of using FRP composites for improving the flexural resistance of unreinforced hollow concrete masonry walls. The experiments involved testing of six large-scale masonry walls against the out-of-plane loading. The dimensions and detailing of test walls are presented in Fig. 1. The test matrix is summarized in Table 1. The first wall, designated WC, was unstrengthened to be used as control specimen for comparison, whereas the other five walls were strengthened using different schemes of externally bonded unidirectional GFRP laminates. For all strengthened walls, designated W1 to W5, no special treatment was given to the GFRP at the terminating ends, while for FRP-upgraded walls W2, W4 and W5, the fibers were oriented perpendicular to the bed joint to simulate the resistance to flexural tensile stresses that develop under out-of-plane loads. The main parameters studied experimentally were FRP reinforcement ratio and FRP surface area ratio. The FRP reinforcement ratio is calculated later [Eq. (6)]. The FRP surface area ratio is defined as the ratio of the surface area of the FRP reinforcement to the surface area of the masonry wall. Both FRP reinforcement ratios and FRP surface area ratios are listed in Table 1 for the five strengthened wall specimens.

The specimens were tested to simulate the case of the FRP being fully anchored, which may represent practical cases of FRP strengthening a URM wall for out-of-plane loading. For external faces, it may be possible to extend the FRP laminates beyond the edge of the wall to the boundary elements. When FRP laminates are applied to interior faces, they may be anchored to boundary elements in order to mitigate the unwanted end debonding mode of failure.

Wall Construction

The locally available hollow concrete masonry units (CMUs) of $200 \times 200 \times 400$ mm were used for the construction of masonry walls. The net area of the used block was 52,800 mm^2 and its cross-section is as shown in Fig. 2. The dimensions of the walls were $1{,}650 \times 1{,}650$ mm and one block wide. The wall dimensions were selected based on available resources in the laboratory. Since many facilities were constructed using a running or staggered bond, it was necessary to eliminate the effects of bond pattern. The walls were constructed in running bond using full and half stretchers with faceshell bedding. Type S masonry mortar was used. No grouting was done in the hollow blocks and no reinforcement was used. The specimen walls were constructed by expert mason from the local market. After the completion of the wall construction, the walls were allowed to cure for 30 days before the GFRP installation. The GFRP system was bonded to the surface of the walls using the traditional wet lay-up process. The pretreatment of the wall included sandblasting, brushing, and cleaning to ensure proper bonding of GFRP with the wall.

Material Properties

Tests were conducted to characterize the engineering properties of the constituent materials. The mix proportion of cement mortar used in the construction of walls was 1:3 (cement:fine sand) with water-to-cement ratio of 0.6. The compressive strength of mortar was determined using 50-mm cubes that were tested in accordance with ASTM C109/C109M (ASTM 2008a). The 28-day average compressive strength of the mortar was 13.8 MPa; therefore, the mortar may be classified as Type S. The compressive strength of masonry was 6.1 MPa, which was determined using three CMU prisms. In the present study, GFRP sheets with unidirectional fibers were used for strengthening the masonry walls. The coupon samples of GFRP were cut from the sheets and tested in accordance with ASTM D3039/3039M (ASTM 2008b) to determine the average mechanical properties of the GFRP composite. The thickness per one layer of the GFRP composite was determined to be 1.85 mm. The ultimate tensile strength, modulus of elasticity, and rupture strain of the GFRP laminates in the direction of fibers were 325 MPa, 16.9 GPa, and 2.1%, respectively.

Test Setup

The wall specimens were tested to failure using an airbag and reaction frame to obtain a uniform load on the wall (Fig. 3). The walls were placed in a horizontal position and tested as one-way slabs with span direction perpendicular to the mortar bed joints. The test specimen was supported by two steel rods, which acted as roller supports (restraining only the vertical movement during loading and allowing for rotation and horizontal movement). A calibrated pressure transducer was used to measure the applied pressure during the tests. The pressure applied to the wall was controlled by regulating the pressure in the airbag. The out-of-plane deflections of wall were measured using linear variable differential transducers (LVDTs), and electrical resistance strain gauges were used for recording FRP strains. The pressure transducer, LVDTs and strain gauges were provided by Tokyo Sokki Kenkyujo (TML), Japan. Fig. 4 shows the locations of different sensors used for test walls.

Downloaded from ascelibrary.org by King Saud University on 01/12/21. Copyright ASCE. For personal use only; all rights reserved.

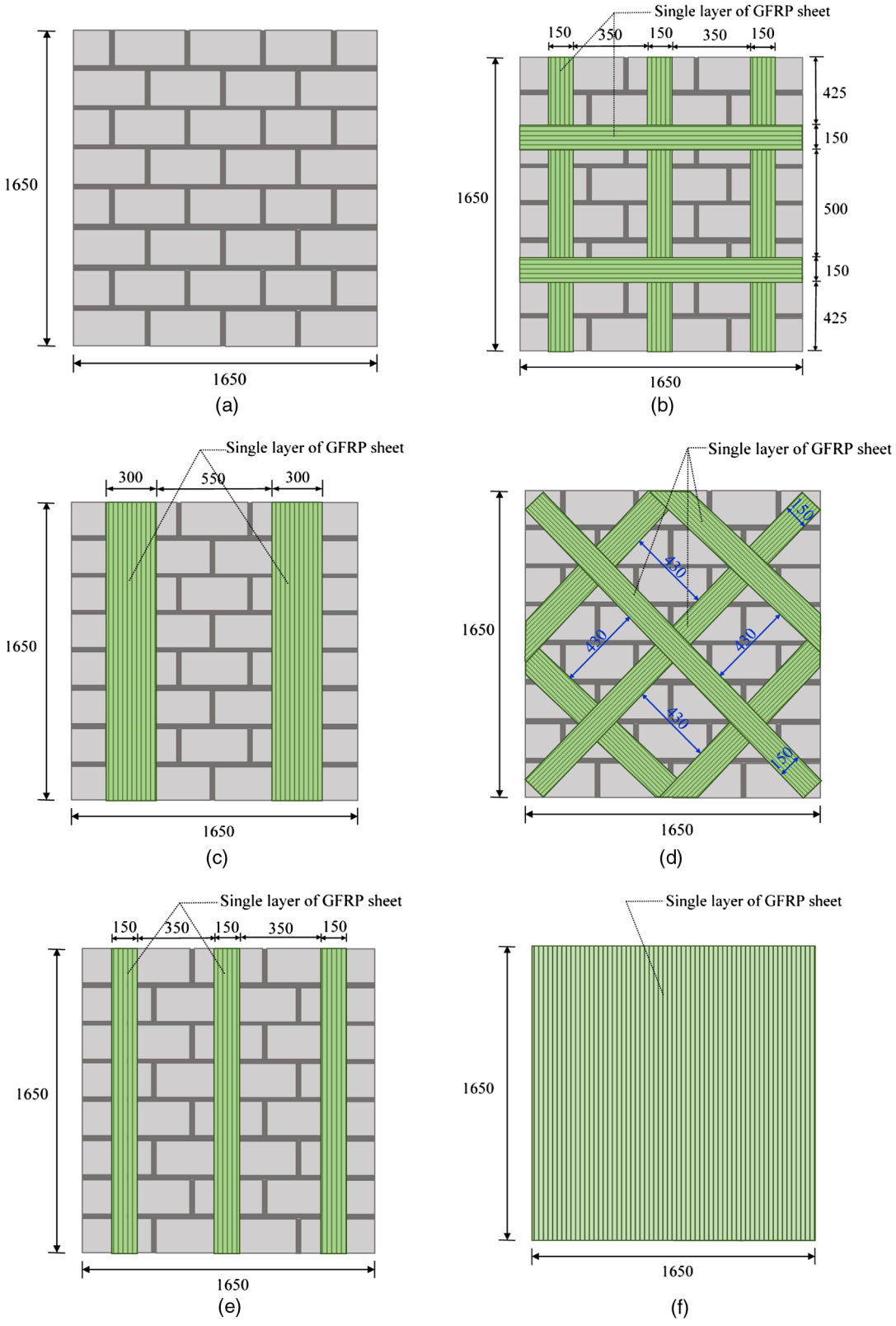

Fig. 1. Details of test walls: (a) Wall WC; (b) Wall W1; (c) Wall W2; (d) Wall W3; (e) Wall W4; (f) Wall W5 (note: all dimensions are in mm)

Test Results

Modes of Failure

The modes of failure of walls recorded during experiments are summarized in Table 2 for all test walls. Fig. 5 presents the failure modes of walls for representative samples of test specimens. For the control unstrengthened specimen WC, the failure of wall initiated near the midspan with the appearance of a crack in the mortar bed that propagated along the width of the wall. With the increase in load, the cracks increased leading to the sudden failure of the wall. As mentioned earlier, the FRP laminates were fully extended

Downloaded from ascelibrary.org by King Saud University on 01/12/21. Copyright ASCE. For personal use only; all rights reserved.

Table 1. Test Matrix

Wall identified	GFRP strengthening system							Number of specimens
	Fiber orientation[a]	Number of layers	Number of strips	Strip width (mm)	Center-to-center strip spacing (mm)	Reinforcement ratio (%)	Surface area ratio (%)	
WC				Control specimen				1
W1	0°	1	3	150	500	0.27	45.5	1
	90°	1	2	150	650	—	—	—
W2	0°	1	2	300	850	0.37	36.4	1
W3	45°	1	3	150	580	0.13[b]	51.4	1
	−45°	1	3	150	580	—	—	—
W4	0°	1	3	150	500	0.27	27.3	1
W5	0°	1	1	1,650	—	1.01	100.0	1
Total number of specimens						—	—	6

[a]Measured with respect to the span direction of the test specimen.
[b]Calculated using equivalent FRP area at midspan resolved in the span direction.

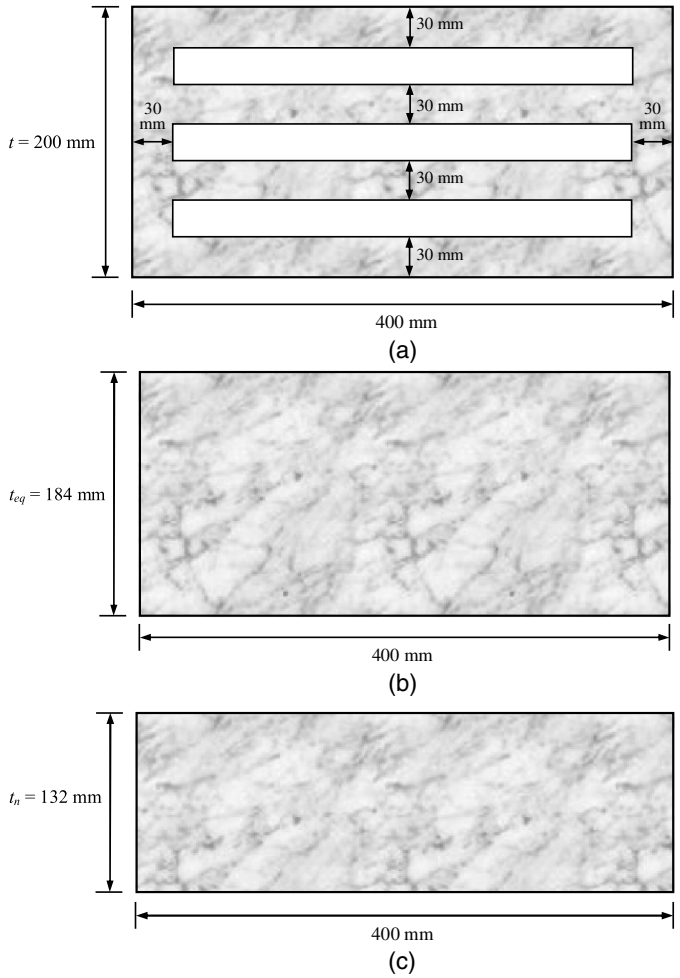

Fig. 2. Typical CMU block used: (a) actual section dimensions; (b) equivalent solid section for flexural capacity calculations; (c) equivalent solid section for shear strength calculations

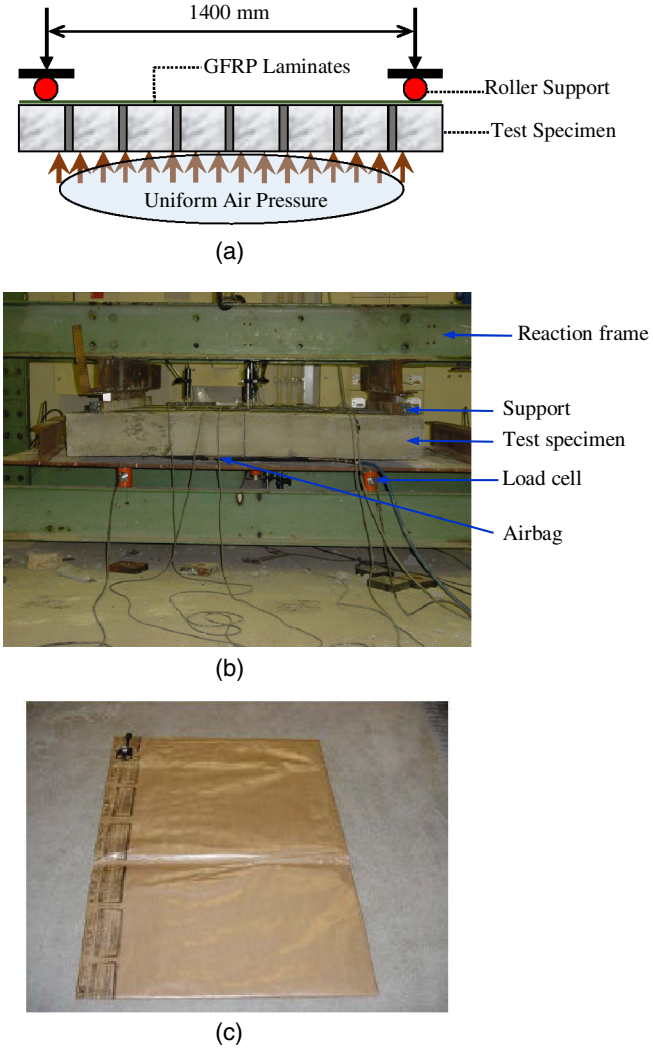

Fig. 3. Test setup: (a) typical air pressure loading; (b) test rig; (c) airbag

to the end of the FRP-strengthened specimens; therefore, the end debonding failure mode was mitigated and all strengthened walls displayed the following modes of failure: (1) flexural failure due to either rupture of the FRP laminates (Wall W3) or debonding of the FRP laminate from the masonry substrate (Walls W1, W2, and W4), and (2) one-way shear failure in the block masonry near the support (Wall W5). Due to its low FRP reinforcement ratio of 0.13%, Wall W3 failed due to the rupture of FRP at the maximum moment region after the development of flexural cracks mainly located at the mortar bed joints [Fig. 5(c)]. However, for Walls W1, W2, and W4, FRP debonding occurred due to shear transfer at the FRP–masonry interface. This debonding was similar to the intermediate crack (IC) debonding encountered in FRP-retrofitted beams and one-way slabs (Elsanadedy et al. 2014, 2015; Lu et al. 2007), and it started from flexural cracks at the maximum moment

Downloaded from ascelibrary.org by King Saud University on 01/12/21. Copyright ASCE. For personal use only; all rights reserved.

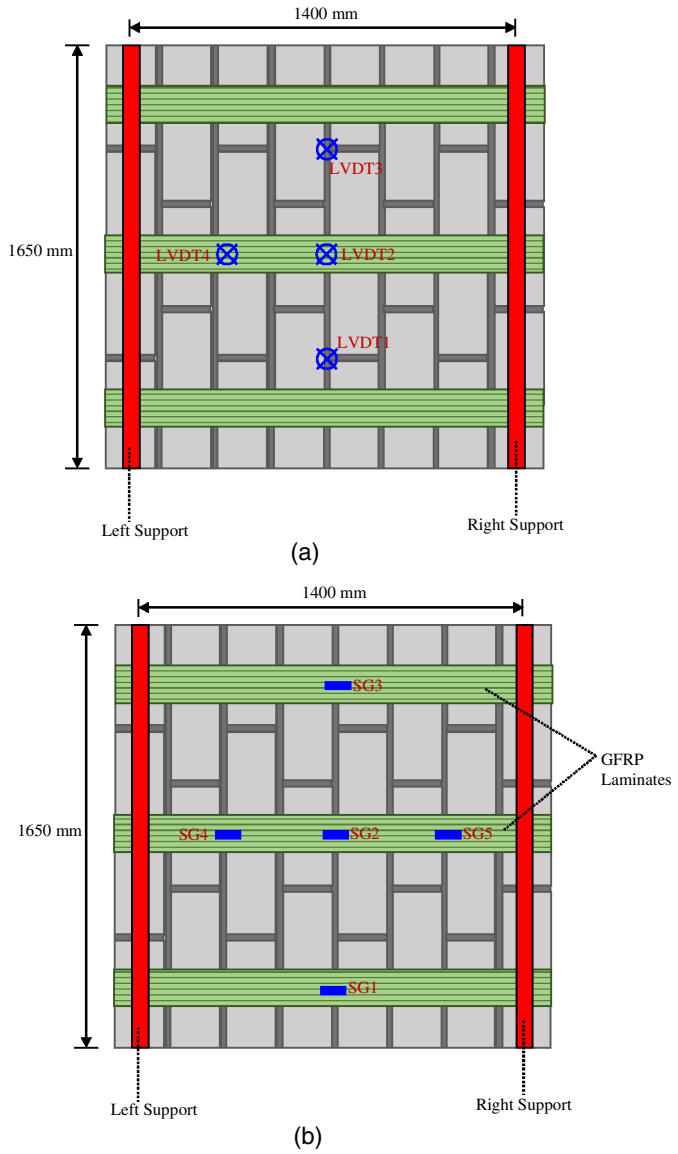

Fig. 4. Instrumentation layout: (a) deflection sensors; (b) strain gauges

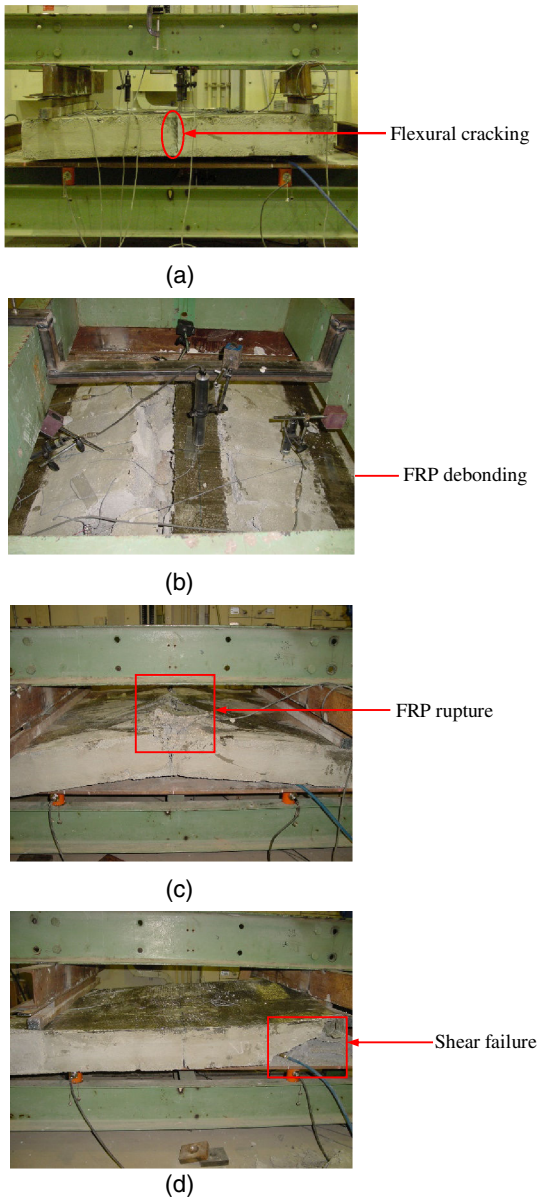

Fig. 5. Mode of failure for representative samples of test walls: (a) control wall WC; (b) Wall W1; (c) Wall W3; (d) Wall W5

Table 2. Summary of Experimental Results for Specimens Tested in This Study

Wall identifier	Ultimate moment (kN · m)	Ultimate midspan deflection (mm)	Maximum FRP strain ($\mu\varepsilon$)	Failure mode
WC	5.8	N/A	—	Flexural failure
W1	36.7	19.2	15,800	FRP debonding
W2	40.6	20.8	13,100	FRP debonding
W3	23.7	17.6	20,400	FRP rupture
W4	38.3	20.2	14,300	FRP debonding
W5	51.9	26.6	4,800	Shear failure

Note: N/A = no available data.

region and then propagated towards the supports. As the tensile strength of masonry is less than that of the epoxy resin, the failure line was in the masonry and part of the concrete block faceshell remained bonded to the FRP sheet [Fig. 5(b)]. For Wall W5, which had a high FRP reinforcement ratio of 1.0%, shear failure occurred near the right support [Fig. 5(d)].

Discussion of Results

Table 2 shows a summary of the test results of all test walls in terms of (1) ultimate moment, (2) ultimate midspan deflection, (3) FRP strain at peak moment, and (4) failure mode. From the table, it is clear that the ultimate moment of the strengthened specimens range from 23.7 to 51.9 kN · m compared to 5.8 kN · m for the control one. This drastic increase in the flexural capacity of retrofitted walls clearly shows the great benefit of the GFRP laminates in transforming the masonry wall from individual concrete blocks to a composite masonry wall of high flexural capacity. It can be further observed from Table 2 that the deformation capacity of the retrofitted walls was also increased drastically after GFRP strengthening, which may bring the importance of GFRP composites in significantly enhancing the ductility capacity of masonry walls exposed to out-of-plane loading in cases of wind or seismic events.

Fig. 6 illustrates moment versus midspan deflection for all wall specimens. The deflection curves for all five strengthened walls reveal a definite response pattern. Two distinct phases of response

Downloaded from ascelibrary.org by King Saud University on 01/12/21. Copyright ASCE. For personal use only; all rights reserved.

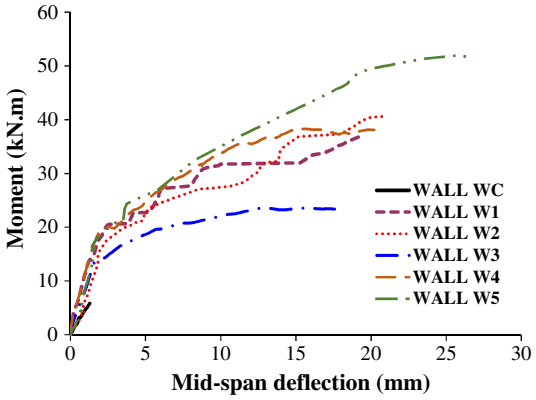

Fig. 6. Moment-deflection curves for test walls

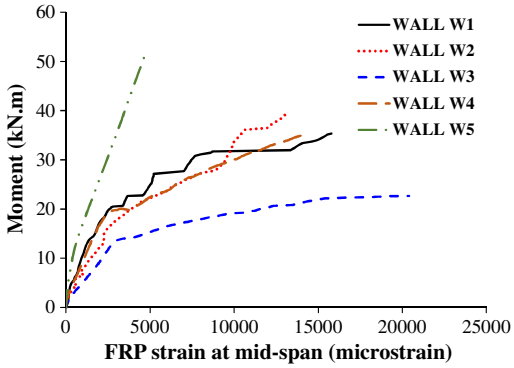

Fig. 7. Moment versus FRP strain curves for test walls

can be seen in Fig. 6. The first phase is almost linear up to 2–3 mm of midspan deflection. During this phase, the mortar reaches its tensile capacity, leading to the initiation of cracking. The separation of a joint or the loss of bond between mortar and the block causes the transfer of load to the next joint, which continues until the joints in the maximum moment region of the wall are completely separated. In the second phase of response, the flexural stiffness of the specimen is reduced to joint separation. At this stage, the flexural stiffness of wall is a function of the FRP reinforcement ratio. This portion of the moment-deflection curve signifies the role of the FRP reinforcement to the behavior of the specimen. However, because the masonry possesses inherent variability, the comparisons, made between the different phases of moment-deflection curves, should not be taken in terms of the exact values but rather taken to indicate the ranges of behavior.

Curves of moment versus FRP strain at midspan are plotted in Fig. 7 for the five FRP-strengthened walls. For specimen Walls W1 to W4, the overall shape of response also reveals two distinct phases. In the first phase until joint separation, the FRP's contribution to the overall capacity of the walls was minimal and the maximum recorded FRP strains ranged from 2,000 to 3,000 $\mu\varepsilon$, as shown in Fig. 7. In the second phase, FRP contribution was more pronounced due to mortar cracking and joint separation, and the FRP strain increased significantly until it reached its rupture value (~20,000 $\mu\varepsilon$) for Wall W3 and values between 13,000 and 16,000 $\mu\varepsilon$ for Walls W1, W2, and W4. However, for Specimen W5 and due to the high amount of FRP reinforcement, the rate of strain increase was considerably less than other specimens, especially in the second phase. The strain increase for Wall W5 was almost linear until it reached its maximum value of 4,800 $\mu\varepsilon$, at which shear failure occurred.

Fig. 8 depicts the effect of FRP reinforcement ratio on the behavior of test walls in terms of (1) percent gain in out-of-plane capacity

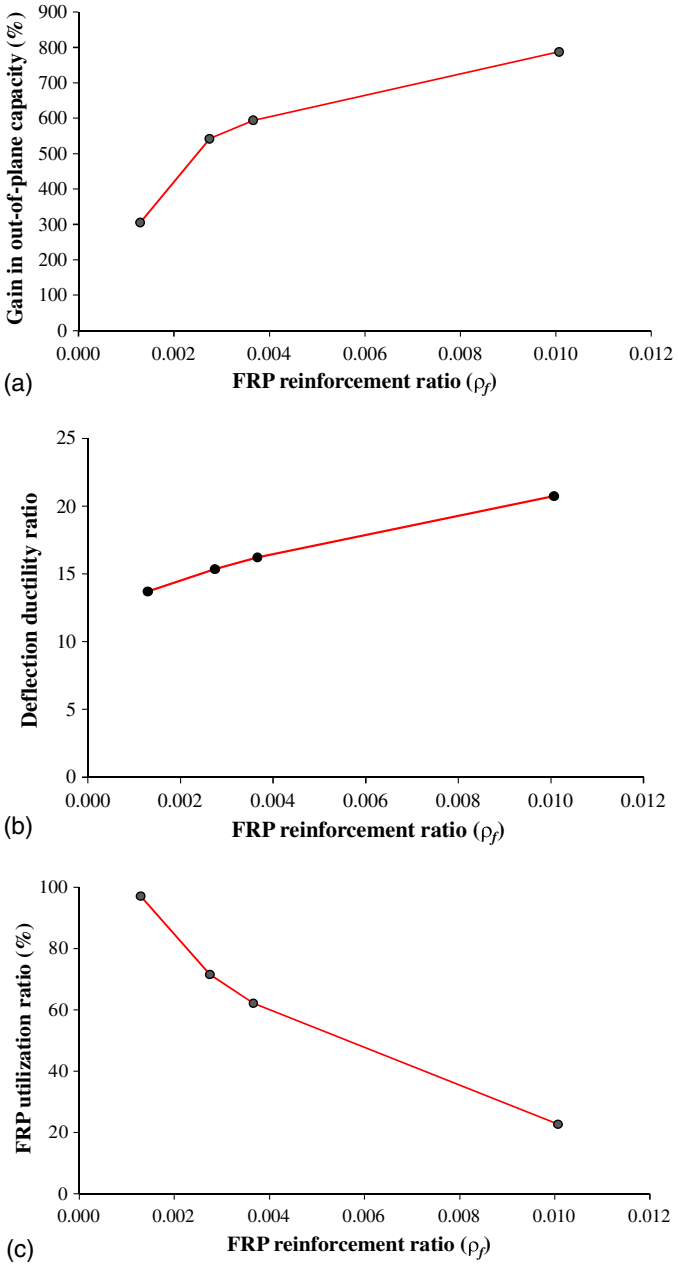

Fig. 8. Effect of FRP reinforcement ratio on performance of test walls: (a) gain in out-of-plane capacity; (b) deflection ductility ratio; (c) FRP utilization ratio

with respect to control specimen, (2) deflection ductility ratio (ratio between ultimate deflection of FRP-strengthened wall to ultimate deflection of unstrengthened specimen), and (3) FRP utilization ratio (ratio between maximum FRP strain and its strain at rupture). As Walls W1 and W4 have the same FRP reinforcement ratio, their output values were averaged in a single value as shown in the curves of Fig. 8. It is demonstrated from Fig. 8(a) that the FRP reinforcement ratio has a major influence on the flexural capacity gain of masonry walls up to reinforcement ratio of 0.27%, after which the effect is reduced. The increase in the FRP reinforcement ratio from 0.13 to 0.27% results in significant gain in the flexural capacity of wall, which increased from 305 to 542%. However, as the reinforcement ratio increases from 0.27 to 1.0%, the flexural capacity increases from 542 to 788%. As depicted in Fig. 8(b), the effect of FRP reinforcement ratio on the deflection ductility ratio is not so pronounced. The ductility ratio increased from 13.7 to 15.4 as the

Downloaded from ascelibrary.org by King Saud University on 01/12/21. Copyright ASCE. For personal use only; all rights reserved.

FRP ratio increased from 0.13 to 0.27%. Fig. 8(c) illustrates that as the FRP reinforcement ratio increases, the FRP utilization ratio decreases. The FRP utilization ratio is significantly reduced from 97 to 23% as the FRP ratio increased from 0.13 to 1.0%.

Analytical Modeling

Velazquez-Dimas and Ehsani (2000) reported that the ultimate-strength method overestimates the flexural capacity of URM walls retrofitted with glass-fiber-composite strips. The materials (i.e., brickwork and composite strips) being brittle, they assumed the behavior of wall as linearly elastic up to failure, which was based on experiments wherein the failure was due to excessive delamination after a large number of loading cycles. They modified the Uniform Building Code (UBC 1991) equations for the midheight deflection of retrofitted walls and recommended that this deflection be limited to $0.007h$ (h = height of wall). Tumialan et al. (2003a) determined the theoretical flexural capacity of an FRP-strengthened masonry based on strain compatibility, internal force equilibrium, and controlling mode of failure. No premature failure was assumed to occur, i.e., rupture of the laminate or crushing of masonry does not govern the wall behavior. A parabolic distribution was used for compressive stresses in the computation of the flexural capacity of the strengthened walls. The maximum usable strain was taken as 0.0035 and 0.0025 for clay and concrete masonry, respectively. The maximum usable strain in the FRP reinforcement for nonputtied and puttied surfaces was recommended as 45 and 65% of the FRP rupture strain, respectively. Tan and Patoary (2004) considered four types of failure in determining the out-of-plane load carrying capacities of wall panels bonded with external FRP systems, namely punching shear through the bricks, crushing of bricks in compression, tensile rupture of the FRP reinforcement, and debonding of FRP reinforcement at the interface. The moment capacity for the strengthened masonry wall was derived based on strain compatibility with a linear strain distribution across the section, and the parabolic compressive stress block of masonry bricks was replaced by an equivalent rectangular stress block. As the flexural bond failure occurs before the flexural compression failure, the strains were assumed to be in the elastic range; thus, for calculating the load corresponding to the bond failure, the stress block was taken as triangular. Mosallam (2007) developed an analytical model to predict the ultimate flexural load of unreinforced red brick walls strengthened with FRP composites. The model was based on section analysis by taking the stress-strain curve for brick–mortar blocks under compression as parabolic up to the maximum compressive strength followed by a linear descending branch. However, the stress block was replaced by an equivalent rectangular stress block.

Hrynyk and Myers (2008) proposed a simplified analytical model to estimate the ultimate out-of-plane capacity for FRP-strengthened URM arching walls. The model was calibrated using experimental data and the results showed good predictions. Hamed and Rabinovitch (2007, 2010) developed an analytical model for flexural capacity of masonry walls strengthened with externally bonded composite materials by incorporating nonlinear behavior of the materials. The model considers the failure criteria that account for crushing and shear failures of the masonry unit and the mortar joints, as well as for rupture and debonding failures of the strengthening system. The nonlinear model was solved using iterative and numerical tools. The comparison of results of analysis with experiments clarified some aspects of the structural response of the strengthened masonry wall and its failure mechanisms under out-of-plane loads. Galal and Sasanian (2010) proposed a method of calculating the deflection of GFRP-reinforced masonry walls using the stress-strain model proposed by Dhanasekar and Shrive (2002). The proposed method incorporated the effect of flexural cracks to the deflections predicted by cracked-section analysis introduced in Intelligent Sensing for Innovative Structures (ISIS), Canada (2001). Within the limited range of GFRP reinforcement ratios covered in the experiments, a capacity diagram was proposed for the design of FRP-reinforced masonry walls. Derakhshan et al. (2013) developed an analytical model to describe the out-of-plane response of one-way spanning URM walls by incorporating the effects of horizontal crack height, masonry compressive strength, and diaphragm support stiffness properties. The prediction of the uncracked wall's resistance and wall crack height in the tested walls produced large errors, which were attributed to errors in masonry bond strength.

In this study, the section analysis procedure was followed in order to compute the out-of-plane capacity of both unstrengthened and GFRP-strengthened URM walls. The procedure is detailed in the following subsections.

Unstrengthened Walls

Proposed Methodology

The ultimate moment capacity of an unstrengthened wall section is assumed equal to its cracking moment, which depends on masonry modulus of rupture [Fig. 9(a)]. In this study, the modulus of rupture, f_r, for masonry elements subjected to out-of-plane loading is assumed as

$$f_r = 0.1 \times \min(f'_m; f'_{\text{mortar}}) \tag{1}$$

where f'_m = compressive strength of masonry; and f'_{mortar} = compressive strength of mortar. The cracking moment is then computed from

$$M_u = M_{cr} = \frac{f_r I_{\text{actual}}}{y_t} = \frac{f_r B t_m^2}{6} \tag{2}$$

where B = total width of masonry wall; and t_m = thickness of masonry wall used in the flexural capacity computations and is given as equal to the total masonry wall thickness, t, for case of solid or fully grouted masonry; and is equal to the equivalent masonry wall thickness, t_{eq}, for case of hollow or ungrouted masonry. The equivalent thickness of wall, t_{eq}, is based on inertia of a hollow masonry block similar to that of equivalent solid block and can be determined from

$$t_{eq} = \sqrt[3]{\frac{12 I_{g(\text{actual})}}{B_b}} \tag{3}$$

where B_b = block width; and $I_{g(\text{actual})}$ = gross inertia of actual block section.

Building Code Requirements for Masonry Structures

The cracking moment capacity of the unstrengthened walls was also computed using the Masonry Standards Joint Committee (MSJC 2011) code specifications for masonry structures. The modulus of rupture was estimated as per Section 3.1.8.2 and Table 3.1.8.2 of the MSJC code (MSJC 2011) and hence, the ultimate moment was calculated using Eqs. (2) and (3).

FRP-Strengthened Walls

Proposed Methodology

The procedure described in this section is only for the FRP strengthening applied to the tension side of the wall because FRP

Downloaded from ascelibrary.org by King Saud University on 01/12/21. Copyright ASCE. For personal use only; all rights reserved.

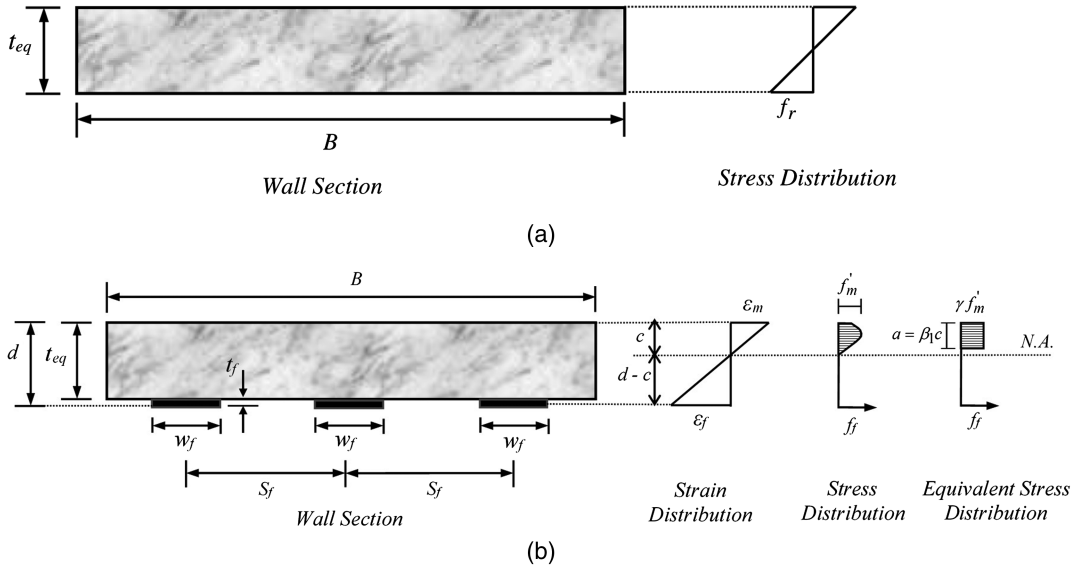

Fig. 9. Internal strain and stress distribution for a typical URM wall section: (a) unstrengthened walls; (b) FRP-strengthened walls

strengthening may not be effective in compression. As discussed previously, the mode of failure of FRP-strengthened walls under out-of-plane loading could be either flexural failure (due to either FRP debonding, FRP rupture or masonry crushing) or shear failure. The ultimate moment of the wall is the least given by flexural and shear failure. The out-of-plane capacity computations corresponding to flexural and shear failures are detailed in the following subsections.

Flexural Capacity Calculations. The proposed procedure is based on the following assumptions:

- A plane section before bending remains plane after bending and thus the flexural strains in masonry and FRP laminate are directly proportional to the distance from the neutral axis;
- The tensile strength of masonry is ignored;
- There is a perfect bond between FRP laminate and the masonry substrate and thus there is no relative slip between the two, until FRP debonding failure occurs; and
- The wall is simply supported on two opposite edges and therefore arching action is absent.

The analysis is based on force equilibrium and strain compatibility. The variation of strain and stress in the FRP-strengthened masonry section under out-of-plane loading is shown in Fig. 9(b). The stress block parameters γ and β_1 for the parabolic variation of compressive stress can be calculated from the following equations (Tumialan et al. 2003b):

$$\beta_1 = 2 - \frac{4\left[\left(\frac{\varepsilon_m}{\varepsilon'_m}\right) - \tan^{-1}\left(\frac{\varepsilon_m}{\varepsilon'_m}\right)\right]}{\left(\frac{\varepsilon_m}{\varepsilon'_m}\right)\ln\left[1 + \left(\frac{\varepsilon_m}{\varepsilon'_m}\right)^2\right]} \tag{4}$$

$$\gamma = 0.90\frac{\ln\left[1 + \left(\frac{\varepsilon_m}{\varepsilon'_m}\right)^2\right]}{\beta_1\left(\frac{\varepsilon_m}{\varepsilon'_m}\right)} \tag{5}$$

where $\varepsilon'_m = 1.71f'_m/E_m$ and $\tan^{-1}(\varepsilon_m/\varepsilon'_m)$ are calculated in radians. The modulus of elasticity of the masonry can be taken as $E_m = 900f'_m$ for concrete masonry and $E_m = 700f'_m$ for clay masonry (MSJC 2011). In this study, the maximum usable strain at the extreme compressive side, ε_{mu}, is assumed to be 0.003 for concrete masonry and 0.0035 for clay masonry (Galati et al. 2005; ACI 2010).

The flexural load capacity of FRP-upgraded masonry walls subjected to out-of-plane loading depends on its failure mode, which may be either masonry crushing, FRP rupture, or debonding. The failure mode of FRP-strengthened walls is decided by comparing the FRP reinforcement ratio of the masonry wall section with the balanced reinforcement ratio, which is the ratio corresponding to the state at which masonry crushing and FRP rupture or debonding occur simultaneously. The FRP reinforcement ratio for a wall section is computed from

$$\rho_f = \frac{A_f}{Bd} \tag{6}$$

where d = effective depth of wall section [$\approx$ total wall thickness, t, in case of solid or fully grouted masonry and $\approx$ effective wall thickness, t_{eq}, given by Eq. (3) in case of hollow masonry]; and A_f = total cross-sectional area of externally bonded FRP laminates, given by

$$A_f = n \times n_s \times w_f \times t_f \tag{7}$$

where n = number of FRP layers; n_s = number of FRP strips; w_f = width of FRP strip; and t_f = thickness per layer of FRP reinforcement. The balanced FRP reinforcement ratio is computed by considering force equilibrium and strain compatibility, thus giving

$$\rho_{fb} = \gamma\beta_1\frac{f'_m}{f_{fe}}\frac{\varepsilon_{mu}}{\varepsilon_{mu} + \varepsilon_{fe}} = \gamma\beta_1\frac{f'_m}{f_{fe}}\frac{E_f\varepsilon_{mu}}{E_f\varepsilon_{mu} + f_{fe}} \tag{8}$$

where β_1 and γ = stress block parameters calculated using Eqs. (4) and (5), taking $\varepsilon_m = \varepsilon_{mu}$ and f_{fe} = effective FRP stress at debonding, expressed as $f_{fe} = E_f\varepsilon_{fe}$, where E_f = tensile modulus of elasticity for FRP laminates and ε_{fe} = effective FRP strain, which is the same as debonding strain of FRP reinforcement. In this research, the FRP debonding strain is estimated using the following equation, which was proposed by Elsanadedy et al. (2015) for FRP-strengthened reinforced concrete one-way slabs:

$$\varepsilon_{fe} = \varepsilon_{fd} = 8.1 \times (\alpha_s)^{-1.674} \leq \varepsilon_{fu} \tag{9}$$

Downloaded from ascelibrary.org by King Saud University on 01/12/21. Copyright ASCE. For personal use only; all rights reserved.

where ε_{fu} = strain at rupture for FRP laminates; and α_s = stiffness parameter, which is a measure of the FRP stiffness with respect to masonry compressive strength and is used for estimating the FRP debonding strain. This parameter is given by the following empirical formula:

$$\alpha_s = \frac{1}{\beta_w}\sqrt{\frac{nE_f t_f}{f'_m}} \tag{10}$$

where β_w = FRP-to-masonry width ratio factor, which affects the bond–slip parameters (Lu et al. 2005) and it is given by

$$\beta_w = \sqrt{\frac{2.25 - w_f/S_f}{1.25 + w_f/S_f}} \tag{11}$$

where S_f = center-to-center spacing of FRP strips [Fig. 9(b)]. If the FRP reinforcement ratio is less than the balanced reinforcement ratio ($\rho_f < \rho_{fb}$), FRP debonding or rupture occurs. Otherwise, when $\rho_f > \rho_{fb}$, the crushing of masonry governs the failure of wall. For each case, the ultimate flexural capacity may be estimated as follows:

- For $\rho_f > \rho_{fb}$, the failure of wall is initiated by crushing of the masonry, and the stress variation in the masonry can be approximated by an equivalent rectangular stress block with the parameters β_1 and γ, which can be estimated from Eqs. (4) and (5) using $\varepsilon_m = \varepsilon_{mu}$. In this case, $\beta_1 = 0.82$ and 0.84 for clay and concrete masonry, respectively; whereas, $\gamma = 0.85$ for both masonry types. Based on equilibrium of internal forces and strain compatibility, the stress in the FRP reinforcement can be estimated from

$$f_f = \left[\sqrt{\left(\frac{E_f\varepsilon_{mu}}{2}\right)^2 + \frac{\gamma\beta_1 f'_m E_m \varepsilon_{mu}}{\rho_f}} - \frac{E_f\varepsilon_{mu}}{2}\right] \le f_{fe} \tag{12}$$

  Hence, the neutral axis depth can be calculated from

$$a = \frac{\rho_f d f_f}{\gamma f'_m} \tag{13}$$

  The ultimate flexural strength can be then determined from the following equation:

$$M_u = \rho_f B d f_f\left(d - \frac{a}{2}\right) \tag{14}$$

- For $\rho_f < \rho_{fb}$, the failure of the masonry wall is initiated by debonding or rupture of the FRP laminates, and the parameters of equivalent stress block depend on the level of maximum flexural strain reached in the masonry wall. An iterative procedure is to be followed in order to compute the parameters of equivalent stress block. There are four unknowns involved in the analysis, namely, the neutral axis depth, c; the compressive strain of masonry at failure, ε_m; and the equivalent stress block parameters β_1 and γ. The neutral axis depth is initially assumed equal to that at the balanced condition, c_b, given by

$$c_b = \left(\frac{\varepsilon_{mu}}{\varepsilon_{mu} + \varepsilon_{fe}}\right)d \tag{15}$$

  Then, the masonry compressive strain at failure ε_m can be estimated from

$$\varepsilon_m = \varepsilon_{fe}\left(\frac{c}{d-c}\right) \le \varepsilon_{mu} \tag{16}$$

  The stress block parameters β_1 and γ can be then computed using Eqs. (4) and (5) and the neutral axis depth can be recalculated using

$$c = \frac{\rho_f d E_f \varepsilon_{fe}}{\gamma\beta_1 f'_m} \tag{17}$$

  This procedure is repeated until the difference in the neutral axis depth, c, can be ignored. Hence, the ultimate flexural capacity can be computed from

$$M_u = \rho_f B d E_f \varepsilon_{fe}\left(d - \frac{\beta_1 c}{2}\right) \tag{18}$$

Shear Strength Calculations. The ultimate moment calculated in the preceding section for flexural response of FRP-upgraded masonry wall need to be compared and limited by the one associated with shear failure. If a high FRP reinforcement ratio is used for strengthening, the failure of the wall can be controlled by shear rather than flexure. Since the FRP reinforcement is externally bonded onto the masonry surface, its contribution to the shear strength is ignored and the ultimate shear capacity will be given by the masonry alone. In this study, it is proposed to compute the shear strength of the masonry walls subjected to out-of-plane loading as follows.

For hollow or ungrouted masonry units, the shear strength may be estimated using Section 3.2.4 of the *Building code requirements for masonry structures* (MSJC 2011), in which

$$V_u = 0.39A_n \quad (\text{N, mm}) \tag{19}$$

where A_n = net cross-sectional area of masonry wall = Bt_n where B = total wall width and t_n = equivalent wall thickness based on net area. However, for solid or fully grouted masonry units, the shear strength may be estimated from the following proposed equation:

$$V_u = 0.1875\sqrt{f'_m}A_n \ge 0.39A_n \quad (\text{N, mm}) \tag{20}$$

The preceding equation is the same as Eqs. (3)–(23) of the MSJC (2011) with zero axial load and conservatively putting the ratio of $M_u/V_u d = 1.0$. The ultimate moment corresponding to shear strength can be then estimated from the following formula:

$$M_u = \begin{cases} V_u a & \text{for case of concentrated loads} \\ \dfrac{V_u[0.5L(0.5u+t) - 0.5(0.5u+t)^2]}{0.5L - 0.5u - t} & \text{for case of uniform load} \end{cases} \tag{21}$$

where a = shear span; L = wall span measured center-to-center between supports; and u = width of support. In the preceding equation and in case of uniform load, the support reaction is assumed to introduce compression into the end region of the wall and hence the critical section for shear is assumed at a distance t from the support face, where t = total wall thickness.

American Concrete Institute 440.7R-10 Guidelines

The American Concrete Institute (ACI) guidelines 440.7R-10 (ACI 2010) were also followed to compute the out-of-plane capacity of FRP-upgraded walls. Since the objective is to determine the flexural load capacity of test walls, the strength reduction factor is taken

Downloaded from ascelibrary.org by King Saud University on 01/12/21. Copyright ASCE. For personal use only; all rights reserved.

as unity (i.e., $\phi = 1$). In computing the flexural capacity, the FRP debonding strain was given as

$$\varepsilon_{fd} = 0.45\varepsilon_{fu} \leq \frac{260}{nt_f E_f} \quad \text{(N, mm)} \tag{22}$$

where ε_{fu} = strain at rupture for FRP laminates. In addition, the maximum allowable compressive strain in concrete masonry is taken as 0.0025. As per the ACI 440.7R-10, the stress block parameters γ and β_1 are each equal to 0.8 when crushing of the masonry is the governing failure mode. However, if FRP rupture or debonding occurs before crushing of the masonry, methods considering a nonlinear stress-strain distribution can be employed to estimate γ and β_1. In this study, Eqs. (4) and (5) shown earlier were used. In the flexural capacity calculations using the ACI 440.7R-10 guidelines, the equivalent masonry wall thickness, t_{eq}, detailed previously as given in Eq. (3), was utilized for case of hollow or ungrouted masonry. For shear strength calculations, the ACI 440.7R-10 guidelines recommend the use of Section 3.2.4 of the MSJC (2011) for either solid or hollow masonry, in which Eq. (19) is used.

Validation of Analytical Modeling

The validation of the analytical modeling procedure was performed by comparing the results of the experiments of the present study and other tests carried out by different researchers with the analytical results proposed in this research. Wall W3 was not included in the comparison with the analytical model because the FRP was loaded off-axis. Besides the five walls tested in the present study, another 42 masonry wall specimens subjected to out-of-plane loading and tested by different researchers (Al-Salloum and Almusallam 2005; Mosallam 2007; Tumialan et al. 2002; Anil et al. 2012; Valluzzi et al. 2014; Hamilton and Dolan 2001; Albert et al. 2001) were used for calibrating the analytical modeling. Tables 3 and 4 present the details and dimensions of URM walls, including their designation, tested by other researchers. Out of the 42 specimens listed in Tables 3 and 4, three were unstrengthened; whereas 39 walls were upgraded with different FRP systems. Thus, the analytical modeling was validated with the help of the experimental database comprising 4 unstrengthened and 43 FRP-upgraded masonry walls. In addition, only those experimental tests were chosen for which most geometric and material characteristics were available. The experimental database used in the analytical model validation covers a wide range of the influencing parameters {masonry units include hollow concrete blocks and solid clay bricks as well as hollow clay bricks; masonry compressive strengths range from 1.8 to 17.1 MPa; FRP reinforcement ratios ranges from $\rho_f = 0.13\rho_{fb}$ to $\rho_f = 2.48\rho_{fb}$ and FRP stiffness parameter [defined earlier in Eq. (10)] ranges from $\alpha_s = 12.7$ to $\alpha_s = 93.2$}. Summary of the test results of 42 specimens tested by other researchers are listed in Tables 5–7. The analytical results are discussed in the following subsections.

Unstrengthened Walls

Table 5 enlists the comparison between the analytical and experimental results for unstrengthened specimens in terms of ultimate moment capacity. The experimental results were compared versus both the proposed and MSJC (2011) methodologies. Statistical indicators for the experimental to predicted ultimate moment are given also in Table 5 in terms of mean (m), standard deviation (SD), and coefficient of variation (CV). From the table, it is obvious

Table 3. Details and Dimensions of URM Walls Tested by Other Researchers

Wall identifier	Masonry type	Dimension of block (or brick) units (mm)	Wall dimensions (mm)			f'_m (MPa)	f'_{mortar} (MPa)	Load	
			L	B	t			Type	a (mm)
Walls tested by Al-Salloum and Almusallam (2005)									
O-1, O-2S	H-CO-BL	400 × 200 × 200	1,400	1,450	200	5.7	13.8	4.p.b	625
Walls tested by Mosallam (2007)									
WCONT-U, WC-RET-02, WC-RET-090, WE- RET-02	S-CL-BR	203 × 102 × 57	2,290	2,640	102	16	21.4	Uniform	—
Walls tested by Tumialan et al. (2002)									
COG3R, COG5, COG5R, COG7, COG9, COG12, COA3, COA5, COA7, COA9, COA12	H-CO-BL	305 × 203 × 102	1,120	610	102	10.5	7.6	4.p.b	457
CLG3, CLG5, CLG7, CLG7R, CLA3, CLA5, CLA7, CLA9	H-CL-BR	203 × 102 × 64	1,120	610	102	17.1	7.6	4.p.b	457
Walls tested by Anil et al. (2012)									
Specimen-1, Specimen-8, Specimen-10	H-CL-BR	185 × 185 × 135	1,400	1,100	135	2.5	5.4	4.p.b	410
Walls tested by Valluzzi et al. (2014)									
Carbon FRP, Basalt FRP, Flax FRP	H-CL-BR	250 × 250 × 120	1,100	390	120	1.8	4.1	4.p.b	418
Walls tested by Hamilton and Dolan (2001)									
S2	H-CO-BL	400 × 200 × 200	1,780	610	200	14.5	N/A	Uniform	—
S3, S4	H-CO-BL	400 × 200 × 200	1,580	610	200	10.9	N/A	Uniform	—
T1	H-CO-BL	400 × 200 × 200	4,600	1,220	200	13.7	N/A	Uniform	—
T2	H-CO-BL	400 × 200 × 200	4,600	1,220	200	15	N/A	Uniform	—
Walls tested by Albert et al. (2001)									
ICST8, ICST10, ICST11,	H-CO-BL	397 × 193 × 193	3,700	1,210	193	13.4	14.7	4.p.b	1,200
MCS6, MCST4, MGST5	H-CO-BL	390 × 190 × 190	3,700	1,200	190	7.3	12.3	4.p.b	1,200

Note: a = shear span of test specimen; B = width of wall specimen; f'_m = compressive strength of masonry; f'_{mortar} = compressive strength of mortar; H-CO-BL = hollow concrete blocks; H-CL-BR = hollow clay bricks; L = span of wall specimen; S-CL-BR = solid clay bricks; t = thickness of wall specimen; 4.p.b = four-point bending.

Downloaded from ascelibrary.org by King Saud University on 01/12/21. Copyright ASCE. For personal use only; all rights reserved.

Table 4. Properties of FRP Composite for URM Walls Tested by Other Researchers

Wall identifier	Type	n	θ	t_f (mm)	n_s	w_f (mm)	S_f (mm)	E_f (GPa)	f_{fu} (MPa)	ε_{fu}
Walls tested by Al-Salloum and Almusallam (2005)										
O-1						Control specimen				
O-2S	GFRP	1	0°	1	1	1,450	—	30	540	0.018
Walls tested by Mosallam (2007)										
WCONT-U						Control specimen				
WC-RET-02	CFRP	2	0°	0.58	1	2,640	—	103	1,250	0.013
WC-RET-090	CFRP	1	0°	0.58	1	2,640	—	103	1,250	0.013
	CFRP	1	90°	0.58	1	2,640	—	103	1,250	0.013
WE- RET-02	GFRP	3	0°	1.14	1	2,640	—	18.5	425	0.022
Walls tested by Tumialan et al. (2002)										
COG3R	GFRP	1	0°	0.35	1	76	—	92.9	1,690	0.018
COG5, COG5R	GFRP	1	0°	0.35	1	127	—	92.9	1,690	0.018
COG7	GFRP	1	0°	0.35	1	178	—	92.9	1,690	0.018
COG9	GFRP	1	0°	0.35	1	229	—	92.9	1,690	0.018
COG12	GFRP	1	0°	0.35	1	305	—	92.9	1,690	0.018
COA3	AFRP	1	0°	0.28	1	76	—	115	1,880	0.016
COA5	AFRP	1	0°	0.28	1	127	—	115	1,880	0.016
COA7	AFRP	1	0°	0.28	1	178	—	115	1,880	0.016
COA9	AFRP	1	0°	0.28	1	229	—	115	1,880	0.016
COA12	AFRP	1	0°	0.28	1	305	—	115	1,880	0.016
CLG3	GFRP	1	0°	0.35	1	76	—	92.9	1,690	0.018
CLG5	GFRP	1	0°	0.35	1	127	—	92.9	1,690	0.018
CLG7, CLG7R	GFRP	1	0°	0.35	1	178	—	92.9	1,690	0.018
CLA3	AFRP	1	0°	0.28	1	76	—	115	1,880	0.016
CLA5	AFRP	1	0°	0.28	1	127	—	115	1,880	0.016
CLA7	AFRP	1	0°	0.28	1	178	—	115	1,880	0.016
CLA9	AFRP	1	0°	0.28	1	229	—	115	1,880	0.016
Walls tested by Anil et al. (2012)										
Specimen-1						Control specimen				
Specimen-8	CFRP	1	0°	0.12	3	100	450	231	4,100	0.017
—	CFRP	1	90°	0.12	3	100	600	231	4,100	0.017
Specimen-10	CFRP	1	0°	0.12	3	50	350	231	4,100	0.017
—	CFRP	1	90°	0.12	5	50	325	231	4,100	0.017
Walls tested by Valluzzi et al. (2014)										
Carbon FRP	CFRP	1	0°	0.17	1	50	—	240	3,500	0.015
Basalt FRP	BFRP	1	0°	0.14	1	50	—	80	1,700	0.021
Flax FRP	FFRP	1	0°	0.19	1	50	—	45	622	0.024
Walls tested by Hamilton and Dolan (2001)										
S2, S3, S4	GFRP	1	0°	1	1	70	—	23.3	350	0.015
T1	GFRP	2	0°	1	2	70	610	23.3	350	0.015
T2	GFRP	1	0°	1	2	140	610	23.3	350	0.015
Walls tested by Albert et al. (2001)										
ICST8	CFRP	2	0°	0.73	2	250	590	47.5	581	0.013
ICST10	CFRP	1	0°	0.73	2	125	879	47.5	581	0.013
ICST11	CFRP	1	0°	0.73	2	250	590	47.5	581	0.013
MCS6	CFRP	1	0°	1.27	4	50	240	185	2,750	0.015
MCST4	CFRP	1	0°	0.73	2	250	590	47.5	581	0.013
MGST5	GFRP	1	0°	1.81	2	250	590	17.8	373	0.021

Note: E_f = tensile modulus of elasticity of FRP material; f_{fu} = tensile strength of FRP material; n = number of plies of FRP reinforcement; n_s = number of FRP strips; S_f = center-to-center spacing between FRP strips; t_f = thickness of one ply of FRP reinforcement; w_f = width of FRP strip; θ = fiber orientation angle with respect to the span direction of the specimen; ε_{fu} = rupture strain of FRP material.

Downloaded from ascelibrary.org by King Saud University on 01/12/21. Copyright ASCE. For personal use only; all rights reserved.

that the proposed model is better when compared to the MSJC model in predicting the flexural capacity of unstrengthened masonry walls subjected to out-of-plane loading.

FRP-Strengthened Walls

Comparison between the experimental and analytical results are summarized in Tables 6 and 7 for FRP-strengthened walls. The experimental results were compared versus both the proposed as well as the ACI 440.7R-10 models. The ratios of the experimental-to-predicted ultimate capacity are calculated as shown in Table 6 for the 43 FRP-strengthened walls. From Table 6, it is evident that the proposed model is more accurate than the ACI model as it successfully predicted the failure modes for 42 specimens (which represent 100% of the specimens with known failure modes); whereas the ACI model was not successful in predicting the mode of failure for 13 specimens (31% of the data). The ratios of the experimental-to-predicted FRP strain at peak load are listed in Table 7 for 12

Table 5. Comparison of Experimental and Analytical Results for Unstrengthened Wall Specimens

Wall identifier	Ultimate moment (kN · m)				
	Experimental	Proposed	MSJC (2011)	Experimental/ proposed	Experimental/ MSJC
WC	5.8	5.6	4.0	1.04	1.46
O-1	5.3	4.9	3.5	1.07	1.51
WCONT-U	11.2	9.8	3.2	1.15	3.56
Specimen-1	0.4	0.4	0.6	0.87	0.66
Mean				1.03	1.80
SD				0.12	1.24
CV (%)				11.2	68.9

specimens only, since the experimental FRP strains were not available for the rest of the walls. In addition, statistical parameters in terms of mean (m), standard deviation (SD), coefficient of variation (CV), and 5% percentile are listed in Table 7 for the tested-to-predicted FRP strains at peak load. It is depicted from the table that the proposed model predicts well the peak FRP strains, which proves the accuracy of Eq. (9). Yet, the ACI model is less accurate due to its high values for m, SD, and CV. It also significantly overestimated the peak FRP strains for two specimens.

Statistical indicators of the experimental-to-predicted ultimate moment capacity in terms of mean (m), standard deviation (SD), coefficient of variation (CV), 5% percentile, minimum, and

Downloaded from ascelibrary.org by King Saud University on 01/12/21. Copyright ASCE. For personal use only; all rights reserved.

Table 6. Comparison of Experimental and Analytical Moment Capacity for FRP-Upgraded Walls

Wall identifier	Ultimate moment (kN · m)							Failure mode		
		Proposed		ACI		Experimental/ proposed	Experimental/ ACI			
	Experimental	Flexure	Shear	Flexure	Shear			Experimental	Proposed	ACI
W1	36.7	36.8	44.8	20.5	44.8	1.00	1.79	DB	DB	DB
W2	40.6	39.4	44.8	27.1	44.8	1.03	1.50	DB	DB	DB
W4	38.3	36.8	44.8	20.5	44.8	1.04	1.87	DB	DB	DB
W5	51.9	69.8	44.8	53.4	44.8	1.16	1.16	SF	SF	SF
O-2S	52.1	60.2	46.7	46.2	46.7	1.12	1.13	SF	SF	DB
WC-RET-02	128.3	114.4	146.5	62.0	65.9	1.12	2.07	DB	DB	DB
WC-RET-090	104.5	104.6	146.5	63.6	65.9	1.00	1.64	DB	DB	DB
WE- RET-02	129.9	129.5	146.5	63.6	65.9	1.00	2.04	MCR	MCR	DB
COG3R	3.2	3.2	5.4	1.8	5.4	1.02	1.77	DB	DB	DB
COG5	3.3	3.5	5.4	3.0	5.4	0.94	1.11	DB	DB	DB
COG5R	3.4	3.5	5.4	3.0	5.4	0.97	1.14	DB	DB	DB
COG7	3.7	4.5	5.4	4.1	5.4	0.83	0.90	DB	DB	DB
COG9	5.2	7.1	5.4	5.3	5.4	0.96	0.99	SF	SF	DB
COG12	6.1	8.3	5.4	6.9	5.4	1.11	1.11	SF	SF	SF
COA3	2.5	2.4	5.4	1.6	5.4	1.06	1.54	DB	DB	DB
COA5	3.6	3.7	5.4	2.7	5.4	0.98	1.31	DB	DB	DB
COA7	4.7	5.4	5.4	3.8	5.4	0.86	1.23	SF	SF	DB
COA9	5.3	7.1	5.4	4.8	5.4	0.96	1.09	SF	SF	DB
COA12	6.3	8.2	5.4	6.3	5.4	1.16	1.16	SF	SF	SF
CLG3	3.2	3.4	11.1	2.0	11.1	0.94	1.64	DB	DB	DB
CLG5	4.9	5.2	11.1	3.3	11.1	0.94	1.50	DB	DB	DB
CLG7	6.6	6.7	11.1	4.5	11.1	0.99	1.46	DB	DB	DB
CLG7R	7.2	6.7	11.1	4.5	11.1	1.08	1.59	DB	DB	DB
CLA3	2.9	3.0	11.1	1.8	11.1	0.98	1.65	DB	DB	DB
CLA5	5.2	4.6	11.1	3.0	11.1	1.14	1.77	DB	DB	DB
CLA7	6.1	5.9	11.1	4.1	11.1	1.04	1.49	DB	DB	DB
CLA9	8.5	7.2	11.1	5.3	11.1	1.18	1.61	DB	DB	DB
Specimen-8	3.4	3.3	6.7	4.6	6.7	1.03	0.73	DB	DB	DB
Specimen-10	2.4	2.4	6.7	2.8	6.7	0.99	0.86	DB	DB	DB
Carbon FRP	1.3	1.3	1.1	0.9	1.1	1.21	1.49	SF	SF	DB
Basalt FRP	0.9	0.8	1.1	0.4	1.1	1.13	2.22	MCR	MCR	DB
Flax FRP	0.4	0.4	1.1	0.2	1.1	1.01	2.22	FR	FR	DB
S2	4.4	4.6	11.9	1.9	11.9	0.97	2.33	FR	FR	DB
S3	4.0	4.2	11.0	1.9	11.0	0.95	2.12	FR	FR	DB
S4	4.5	4.2	11.0	1.9	11.0	1.06	2.36	FR	FR	DB
T1	18.7	15.7	52.8	6.3	52.8	1.19	2.99	DB	DB	DB
T2	15.2	16.8	52.8	7.6	52.8	0.91	2.01	FR	FR	DB
ICST8	30.1	29.7	40.2	20.5	40.2	1.02	1.47	DB	DB	DB
ICST10	12.5	13.9	40.2	6.3	40.2	0.90	1.99	FR	FR	DB
ICST11	25.0	26.9	40.2	15.3	40.2	0.93	1.64	DB	DB	DB
MCS6	27.8	28.0	35.2	7.6	35.2	0.99	3.66	DB	DB	DB
MCST4	17.3	18.8	35.2	14.3	35.2	0.92	1.21	N/A	DB	DB
MGST5	21.6	18.6	35.2	19.4	35.2	1.16	1.11	DB	DB	DB

Note: DB = FRP debonding; FR = FRP rupture; MCR = masonry crushing; SF = shear failure.

Table 7. Comparison of Experimental and Analytical FRP Strain for FRP-Upgraded Walls

Wall identifier	Max FRP strain ($\mu\varepsilon$)				
	Experimental	Proposed	ACI	Experimental/ proposed	Experimental/ ACI
W1	15,800	15,200	8,300	1.04	1.90
W2	13,100	12,300	8,300	1.06	1.57
W4	14,300	15,200	8,300	0.94	1.72
WC-RET-02	7,100	6,540	2,150	1.09	3.30
WC-RET-090	10,000	9,850	4,310	1.01	2.32
WE- RET-02	10,700	10,300	4,110	1.04	2.61
COG3R	14,900	14,000	8,000	1.07	1.86
COG5R	12,300	10,400	8,000	1.18	1.54
CLG7R	15,400	13,600	8,000	1.13	1.93
Specimen-8	2,660	2,310	7,650	1.15	0.35
Specimen-10	3,020	3,310	7,650	0.91	0.39
ICST11	8,700	9,780	5,510	0.89	1.58
m				1.04	1.76
SD				0.09	0.82
CV (%)				8.8	46.8
5% percentile				0.90	0.37

maximum values, and percentage of data with incorrect failure mode prediction are given in Table 8 for the two predictive models. In addition, the error estimates for the predicted versus experimental ultimate moment are given in Table 9 for the two models. For each model, two sets of error parameters were given; i.e., for the 35 specimens failing in flexure and for all 43 FRP-strengthened specimens. The error-assessment parameters used for checking the accuracy of the models were (1) coefficient of determination (R^2), (2) root-mean square error (RMSE), and (3) mean absolute percent error (MAPE). For checking whether the output is underpredicted or overpredicted, mean percent error (MPE) was calculated. The positive and negative values of MPE indicate overestimation and underestimation, respectively, whereas its desirable value is zero. Two other parameters for the goodness of fit were calculated as the data with absolute error within 15% and the maximum absolute error enveloping 80% of the data. Based on statistical indicators as well as the error estimates, it is evident from Tables 7 and 8 that the proposed prediction model is better than the ACI model in matching the experimental data. The performance of the proposed predictive model is further studied by plotting the relationship between FRP stiffness parameter (α_s) and the ratio of tested-to-predicted ultimate moment as shown in Fig. 10. It is evident from the figure that the proposed model predicted the ultimate moment very accurately for specimens with different failure modes with the ratio of experimental-to-predicted ultimate moment ratio ranging approximately from 0.8 to 1.2.

Proposed Design Protocol

Based on the experimental study of this research and by others, FRP debonding is found to be the most common failure mode for FRP-upgraded masonry walls subjected to out-of-plane loading. If a large amount of FRP reinforcement is provided, shear failure may be observed. In case of designing an externally bonded FRP system for strengthening URM walls against out-of-plane loading such as wind pressure or seismic events, the FRP reinforcement ratio should be limited in order to preclude the unwanted brittle shear failure mode. The experimental database collected in this research was used to come up with an upper limit for the FRP reinforcement ratio that may prohibit shear failure. Fig. 11 shows the relationship between FRP reinforcement ratio in terms of ρ_f/ρ_{fb} and the FRP stiffness parameter (α_s) for the 43 FRP-strengthened walls investigated in this research. From the figure, it is clear that for walls with $\rho_f > 0.8\rho_{fb}$, failure was due to either masonry crushing (for $\rho_f > \rho_{fb}$) or shear. Based on the results of the proposed analytical modeling, the relationship between FRP reinforcement

Table 8. Statistical Parameters for Experimental to Predicted Ultimate Moment Ratio

Model	Mean	SD	CV (%)	5th percentile value	Minimum value	Maximum value	Data with incorrect failure mode prediction (%)	Nonconservative data (%)
Specimens with flexural failure (35 data points)								
Proposed predictive	1.01	0.08	8.2	0.91	0.83	1.19	0	—
ACI 440.7R-10	1.72	0.58	33.7	0.89	0.73	3.66	22.9[a]	—
All specimens (43 data points)								
Proposed predictive	1.02	0.09	9.1	0.90	0.83	1.21	0	—
Proposed design	1.28	0.12	9.1	1.13	1.03	1.51	—	0
ACI 440.7R-10 PREDICTIVE	1.62	0.57	35.1	0.91	0.73	3.66	30.2[a]	—
ACI 440.7R-10 DESIGN	2.68	0.97	36.3	1.46	1.22	6.11	—	0

Note: CV = coefficient of variation; SD = standard deviation.
[a]Calculated for data with known failure modes.

Table 9. Error Estimates for Ultimate Moment Prediction of FRP-Strengthened Walls

Parameter for error estimate	Specimens with flexural failure (35 data points)		All specimens (43 data points)	
	Proposed model	ACI 440.7R-10	Proposed model	ACI 440.7R-10
Mean percent error (MPE)	−0.60	−35.4	−1.44	−31.3
Mean absolute percent error (MAPE)	6.05	39.0	7.03	34.3
Root-mean square error (RMSE)	2.56	18.6	2.69	16.9
Coefficient of determination (R^2)	1.00	0.97	0.99	0.93
Percent data for error within 15%	91.4	11.4	88.4	23.3
Percentage error enveloping 80% data	10.8	52.8	12.4	51.1

Downloaded from ascelibrary.org by King Saud University on 01/12/21. Copyright ASCE. For personal use only; all rights reserved.

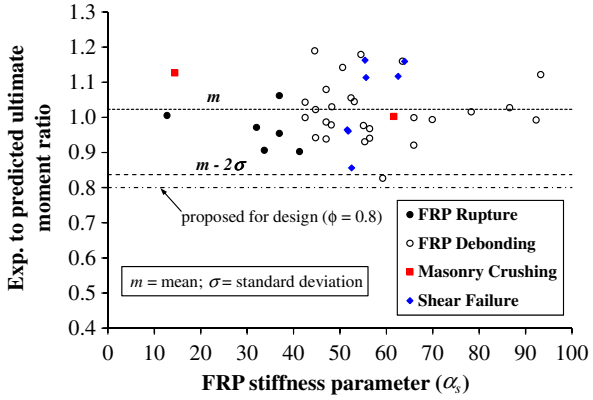

Fig. 10. Performance of proposed analytical model with respect to FRP stiffness parameter (α_s)

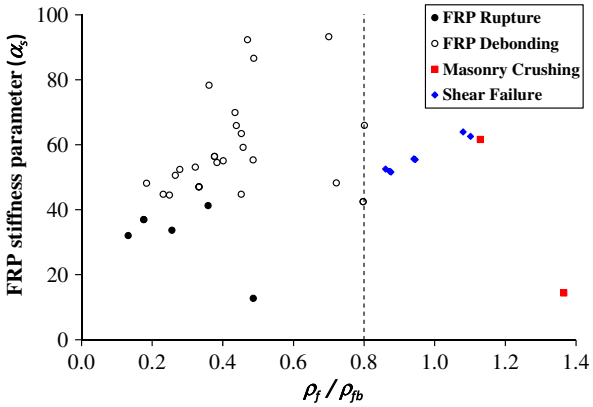

Fig. 11. Effect of FRP reinforcement ratio on failure modes of FRP-upgraded walls (based on experimental results)

ratio in terms of (ρ_f/ρ_{fb}) and flexure-to-shear capacity ratio ($M_{u\text{-}fl}/M_{u\text{-}sh}$) was plotted as shown in Fig. 12. The best-fit regression trendline is also shown in the figure. The trendline has the following equation:

$$\frac{M_{u\text{-}fl}}{M_{u\text{-}sh}} = 1.11\left(\frac{\rho_f}{\rho_{fb}}\right) + 0.12 \tag{23}$$

This equation has $R^2 = 0.80$ (considering all 47 data points for unstrengthened and FRP-strengthened specimens). From the equation and as shown in Fig. 12, it can be inferred that the flexure-to-shear capacity ratio ($M_{u\text{-}fl}/M_{u\text{-}sh}$) equals 1.0 at an FRP reinforcement ratio of $\rho_f = 0.8\rho_{fb}$. Figs. 11 and 12 confirm that for FRP reinforcement ratio of $\rho_f > 0.8\rho_{fb}$, the flexural capacity of the wall may exceed its shear capacity and subsequently, shear failure may occur. In addition to shear failure mitigation, another aspect in the design protocol is the optimum use of the FRP composites for strengthening, which can be expressed via limiting the FRP utilization ratio (defined previously). Considering only the analytical results for the 33 specimens failing by either FRP rupture or FRP debonding, the FRP stiffness parameter (α_s) was plotted against the FRP utilization ratio as presented in Fig. 13. From the figure, it is evident that the FRP stiffness parameter (α_s) should not exceed 60 in order to utilize at least 50% of the FRP strength.

As shown previously in Table 8, the proposed prediction model does not fulfill the requirement of a 5% percentile by having a value less than unity. This further highlights the requirement of a design

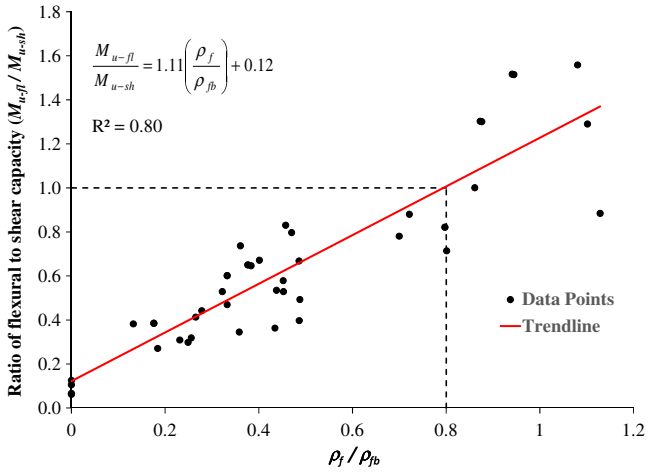

Fig. 12. Effect of FRP reinforcement ratio on flexural to shear capacity ratio of URM walls (based on analytical results)

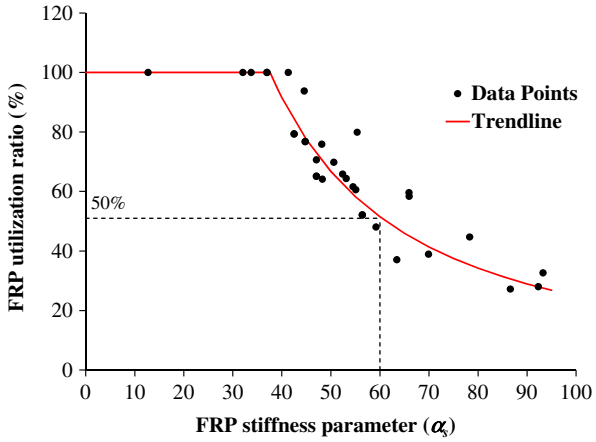

Fig. 13. Effect of FRP stiffness parameter (α_s) on FRP utilization ratio of FRP-upgraded walls (based on analytical results)

model. The design knockdown factor for moment capacity calculations shall be based on the statistical lower bounds of the ratio of experimental to predicted ultimate moment in terms of *mean* – 2σ, where σ is the standard deviation. In addition, two more conditions were enforced: no nonconservative data points and a minimum factor of safety of 1.10 for 95% of the data. As apparent from Table 8, the proposed predictive model detailed previously may be converted to the design model by incorporating a reduction factor of 0.80 for both flexural and shear strength calculations. As outlined in the ACI 440.7R-10 (ACI 2010), the ACI predictive model discussed previously can be converted to the design model by implementing strength reduction factors (ϕ) of 0.6 and 0.8 for flexural and shear strength calculations, respectively.

For the evaluation of design models, the ratio of the experimental to the design value of ultimate moment capacity was also determined. Some statistical indicators, namely, mean, coefficient of variation (CV), standard deviation (SD), and 5th percentile, calculated for the two design models are given in Table 8. Percentage of nonconservative data is also reported in the table. For best results, both coefficient of variation and standard deviation should be low, the 5th percentile should be at least 1.10, the mean should be greater than 1.0 but not very large, and the nonconservative data points should be zero. The proposed design model is found to better

Downloaded from ascelibrary.org by King Saud University on 01/12/21. Copyright ASCE. For personal use only; all rights reserved.

demonstrate optimal values of all the statistical indicators used for model assessment. It is evident from Table 8 that the ACI model is very conservative, which could lead to an uneconomic FRP strengthening design with higher reinforcement ratio.

Conclusions

On the basis of experimental and analytical results presented in this research, the following major conclusions can be drawn:

1. Externally bonded FRP composite systems are effective in significantly upgrading the load carrying capacity of URM walls subjected to out-of-plane loading. In addition, the FRP composites are capable of dramatically increasing the out-of-plane deformation capacity of URM walls, which may show the importance of FRP laminates in significantly enhancing the ductility capacity of masonry walls exposed to wind or seismic loading. The effectiveness of FRP composites in enhancing the load and/or deformation capacity of URM walls decreases with the increase of FRP reinforcement ratio. For instance, for specimens tested in this study, the FRP utilization ratio is significantly reduced from 97 to 23% as the FRP ratio increased from 0.13 to 1.0%.
2. FRP debonding is the most common failure mode for FRP-upgraded URM walls subjected to out-of-plane loading. The debonding is initiated at cracks appearing in bending moment and shear force critical zones, then propagates in the direction of decreasing moment to the ends.
3. An analytical model was proposed in this study. A comparison of the model prediction with the experiments of 47 specimens shows that the proposed analytical procedure is suitable to estimate the flexural capacity of the unstrengthened as well as the FRP-strengthened masonry walls subjected to out-of-plane loading. This confirms the validity of the analytical modeling procedures, which may be employed in future studies on URM walls.
4. The procedure of the ACI 440.7R-10 guidelines were also followed to predict the out-of-plane capacity of FRP-upgraded masonry walls using a strength reduction factor (ϕ) of 1.0. In comparison with the experimental results of 43 FRP-strengthened specimens, the ACI model was found to be inaccurate with the ratio of experimental-to-predicted flexural capacity ranging from 0.73 to 3.66. Moreover, the ACI model was not successful in predicting the mode of failure for 13 specimens (31% of the data with known failure modes).
5. In order to design an FRP system for upgrading the out-of-plane capacity of masonry walls, a strength reduction factor (ϕ) of 0.8 is suggested for both flexural and shear strength calculations to convert the proposed analytical model to the design model. Two aspects should be considered in the design protocol. The first aspect is to control the failure mode of strengthened walls via flexure rather than shear. This could be achieved by limiting the FRP reinforcement ratio (ρ_f) to not exceed 80% of its balanced ratio (ρ_{fb}). The second aspect is to optimize the stress ratio of the FRP laminates to be not less than 50% by limiting the FRP stiffness parameter (α_s) to not exceed 60.

Acknowledgments

This research was supported by Deanship of Scientific Research Chairs at King Saud University, Saudi Arabia for MMB Chair of Research and Studies in Strengthening and Rehabilitation of Structures at Civil Engineering Department.

References

ACI (American Concrete Institute). (2010). "Guide for the design and construction of externally bonded fiber-reinforced polymer systems for strengthening unreinforced masonry structures." *ACI 440.7R-10*, Farmington Hills, MI.

Albert, M. L., Elwi, A. E., and Cheng, J. J. R. (2001). "Strengthening of unreinforced masonry walls using FRPs." *J. Compos. Constr.*, 10.1061/(ASCE)1090-0268(2001)5:2(76), 76–84.

Almusallam, T. H., and Al-Salloum, Y. A. (2007). "Behavior of FRP strengthened infill walls under in-plane seismic loading." *J. Compos. Constr.*, 10.1061/(ASCE)1090-0268(2007)11:3(308), 308–318.

Al-Salloum, Y. A., and Almusallam, T. H. (2005). "Load capacity of concrete masonry block walls strengthened with epoxy-bonded GFRP sheets." *J. Compos. Mater.*, 39(19), 1719–1745.

Anil, O., Tatayoglu, M., and Demirhan, M. (2012). "Out-of-plane behavior of unreinforced masonry brick walls strengthened with CFRP strips." *Constr. Build. Mater.*, 35, 614–624.

ASTM. (2008a). "Standard test method for compressive strength of hydraulic cement mortars (using 2-in. or [50-mm] cube specimens)." *ASTM C109/C109M*, West Conshohocken, PA.

ASTM. (2008b). "Standard test method for tensile properties of polymer matrix composite materials." *ASTM D3039/D3039M–08*, West Conshohocken, PA.

ASTM. (2014). "Standard test methods of conducting strength tests of panels for building construction." *ASTM E72*, West Conshohocken, PA.

Dafnis, A., Kolsch, H., and Reimerdes, H. G. (2002). "Arching in masonry walls subjected to earthquake motions." *J. Struct. Eng.*, 10.1061/(ASCE)0733-9445(2002)128:2(153), 153–159.

Derakhshan, H., Griffith, M. C., and Ingham, J. M. (2013). "Airbag testing of multi-leaf unreinforced masonry walls subjected to one-way bending." *Eng. Struct.*, 57, 512–522.

Dhanasekar, M., and Shrive, N. G. (2002). "Strength and deformation of confined and unconfined grouted concrete masonry." *ACI Struct. J.*, 99(6), 819–826.

El-Dakhakhni, W. W., Hamid, A. A., Hakam, Z. H. R., and Elgaaly, M. (2006). "Hazard mitigation and strengthening of unreinforced masonry walls using composites." *Compos. Struct.*, 73(4), 458–477.

Elsanadedy, H., Abbas, H., Al-Salloum, Y., and Almusallam, T. (2014). "Prediction of intermediate crack debonding strain of externally bonded FRP laminates in RC beams and one-way slabs." *J. Compos. Constr.*, 10.1061/(ASCE)CC.1943-5614.0000462, 04014008.

Elsanadedy, H. M., Almusallam, T. H., Alsayed, S. H., and Al-Salloum, Y. A. (2015). "Experimental and FE study on RC one-way slabs upgraded with FRP composites." *KSCE J. Civ. Eng.*, 19(4), 1024–1040.

Galal, K., and Sasanian, N. (2010). "Out-of-plane flexural performance of GFRP-reinforced masonry walls." *J. Compos. Constr.*, 10.1061/(ASCE)CC.1943-5614.0000061, 162–174.

Galati, N., Garbin, E., Tumialan, G., and Nanni, A. (2005). "Design guidelines for masonry structures: Out of plane loads." *Am. Concr. Inst.*, 230, 269–288.

Ghobarah, A., and Galal, K. (2004). "Out-of-plane strengthening of unreinforced masonry walls with openings." *J. Compos. Const.*, 10.1061/(ASCE)1090-0268(2004)8:4(298), 298–305.

Hamed, E., and Rabinovitch, O. (2007). "Out-of-plane behavior of unreinforced masonry walls strengthened with FRP strips." *Compos. Sci. Technol.*, 67(3–4), 489–500.

Hamed, E., and Rabinovitch, O. (2010). "Failure characteristics of FRP-strengthened masonry walls under out-of-plane loads." *Eng. Struct.*, 32(8), 2134–2145.

Hamilton, H. R., III, and Dolan, C. W. (2001). "Flexural capacity of glass FRP strengthened concrete masonry walls." *J. Compos. Constr.*, 10.1061/(ASCE)1090-0268(2001)5:3(170), 170–178.

Hamoush, S. A., McGinley, M. W., Mlakar, P., Scott, D., and Murray, K. (2001). "Out-of-plane strengthening of masonry walls with reinforced composites." *J. Compos. Constr.*, 10.1061/(ASCE)1090-0268(2001)5:3(139), 139–145.

Hrynyk, T. D., and Myers, J. J. (2008). "Out-of-plane behavior of URM arching walls with modern blast retrofits: Experimental results and

Downloaded from ascelibrary.org by King Saud University on 01/12/21. Copyright ASCE. For personal use only; all rights reserved.

analytical model." *J. Struct. Eng.*, 10.1061/(ASCE)0733-9445(2008)134:10(1589), 1589–1597.
ISIS Canada (Intelligent Sensing for Innovative Structures). (2001). "Reinforcing concrete structures with fiber reinforced polymers." *Design manual no. 3*, Winnipeg, MB, Canada.
Kuzik, M., Elwi, A., and Cheng, J. (2003). "Cyclic flexure tests of masonry walls reinforced with glass fiber reinforced polymer sheets." *J. Compos. Constr.*, 10.1061/(ASCE)1090-0268(2003)7:1(20), 20–30.
Lu, X. Z., Teng, J. G., Ye, L. P., and Jiang, J. J. (2005). "Bond-slip models for sheets/plates bonded to concrete." *Eng. Struct.*, 27(6), 920–937.
Lu, X. Z., Teng, J. G., Ye, L. P., and Jiang, J. J. (2007). "Intermediate crack debonding in FRP-strengthened RC beams: FE Analysis and strength model." *J. Compos. Constr.*, 10.1061/(ASCE)1090-0268(2007)11:2(161), 161–174.
Lunn, D. S., and Rizkalla, S. H. (2011). "Strengthening of infill masonry walls with FRP materials." *J. Compos. Constr.*, 10.1061/(ASCE)CC.1943-5614.0000088, 206–214.
Mosallam, A. S. (2002). "Composites in construction." *Handbook of materials selection*, Wiley, New York.
Mosallam, A. S. (2007). "Out-of-plane flexural behavior of unreinforced red brick walls strengthened with FRP composites." *Compos. Part B*, 38(5-6), 559–574.
MSJC (Masonry Standards Joint Committee). (2011). "Building code requirements and specification for masonry structures." *TMS 402/ACI 530/ASCE 5 and TMS 602/ACI 530.1/ASCE 6*, Boulder, CO.
Tan, K. H., and Patoary, M. K. H. (2004). "Strengthening of masonry walls against out-of-plane loads using fiber-reinforced polymer reinforcement." *J. Compos. Constr.*, 10.1061/(ASCE)1090-0268(2004)8:1(79), 79–87.
Triantafillou, T. C. (1998). "Strengthening of masonry structures using epoxy-bonded FRP laminates." *J. Compos. Constr.*, 10.1061/(ASCE)1090-0268(1998)2:2(96), 96–104.
Tumialan, J. G., Galati, N., and Nanni, A. (2003a). "Field assessment of unreinforced masonry walls strengthened with fiber reinforced polymer laminates." *J. Struct. Eng.*, 10.1061/(ASCE)0733-9445(2003)129:8(1047), 1047–1056.
Tumialan, J. G., Galati, N., and Nanni, A. (2003b). "FRP strengthening of UMR walls subject to out-of-plane loads." *ACI Struct. J.*, 100(3), 321–329.
Tumialan, J. G., Morbin, A., Micelli, F., and Nanni, A. (2002). "Flexural strengthening of URM walls with FRP laminates." *3rd Int. Conf. on Composites in Infrastructure (ICCI 2002)*, Dept. of Civil Engineering and Engineering Mechanics, Univ. of Arizona, Tucson, AZ.
UBC (Uniform Building Code). (1991). *Int. Conf. of Building Officials*, Whittier, CA.
Valluzzi, M. R., Porto, F., Garbin, E., and Panizza, M. (2014). "Out-of-plane behaviour of infill masonry panels strengthened with composite materials." *Mater. Struct.*, 47(12), 2131–2145.
Velazquez-Dimas, J. I., and Ehsani, M. R. (2000). "Modeling out-of-plane behavior of URM walls retrofitted with fiber composites." *J. Compos. Constr.*, 10.1061/(ASCE)1090-0268(2000)4:4(172), 172–181.
Velazquez-Dimas, J. I., Ehsani, M. R., and Saadatmanesh, H. (2000). "Out-of-plane behavior of brick masonry walls strengthened with fiber composites." *ACI Struct. J.*, 97(3), 377–387.

Downloaded from ascelibrary.org by King Saud University on 01/12/21. Copyright ASCE. For personal use only; all rights reserved.